

Characterization of Alkyl-Nickel Adducts Generated by Reaction of Methyl-Coenzyme M Reductase with Brominated Acids[†]

Mishtu Dey,^{‡,§} Ryan C. Kunz,^{‡,§} Derek M. Lyons,^{§,||} and Stephen W. Ragsdale^{*,‡,§}

Department of Biochemistry, University of Nebraska, Lincoln, Nebraska 68588, and Simpson College, Indianola, Iowa 50125

Received May 15, 2007; Revised Manuscript Received July 13, 2007

ABSTRACT: Methyl-coenzyme M reductase (MCR) from methanogenic archaea catalyzes the final step in the biological synthesis of methane. Using coenzyme B (CoBSH) as the two-electron donor, MCR reduces methyl-coenzyme M (methyl-SCoM) to methane and the mixed disulfide, CoB-S-S-CoM. MCR contains coenzyme F₄₃₀, an essential redox-active nickel tetrahydrocorphin, at its active site. The active form of MCR (MCR_{red1}) contains Ni(I)-F₄₃₀. When 3-bromopropane sulfonate (BPS) is incubated with MCR_{red1}, an alkyl-Ni(III) species is formed that elicits the MCR_{ps} EPR signal. Here we used EPR and UV–visible spectroscopy and transient kinetics to study the reaction between MCR from *Methanothermobacter marburgensis* and a series of brominated carboxylic acids, with carbon chain lengths of 4–16. All of these compounds give rise to an alkyl-Ni intermediate with an EPR signal similar to that of the MCR_{ps} species. Reaction of the alkyl-Ni(III) adduct, formed from brominated acids with eight or fewer total carbons, with HSCoM as nucleophile at pH 10.0 results in the formation of a thioether coupled to regeneration of the active MCR_{red1} state. When reacted with 4-bromobutyrate, MCR_{red1} forms the alkyl-Ni(III) MCR_{XA} state and then, surprisingly, undergoes “self-reactivation” to regenerate the Ni(I) MCR_{red1} state and a bromocarboxy ester. The results demonstrate an unexpected reactivity and flexibility of the MCR active site in accommodating a broad range of substrates, which act as molecular rulers for the substrate channel in MCR.

Methanogenic archaea are anaerobic microbes that form methane as an end product of their metabolism. Methanogens produce approximately 1 billion tons of methane every year, providing a valuable source of renewable energy. On the other hand, methane is a greenhouse gas that is 20 times more potent than CO₂ and therefore poses potential environmental problems (1). Methyl-coenzyme M reductase (MCR),¹ found in all methanogens, is a nickel-containing enzyme that catalyzes the terminal step in biological methane formation, which is the reduction of methyl-coenzyme M [2-(methylthio)ethane sulfonate (methyl-SCoM)] with the two-electron donor coenzyme B [*N*-7-mercaptoheptanoyl-

threonine phosphate (CoBSH)], to form methane and the heterodisulfide CoB-S-S-CoM (1–3). There is strong evidence that MCR or a MCR-like enzyme also catalyzes the first step in the anaerobic oxidation of methane (4). The active site of MCR contains a redox-active Ni-tetrapyrrolic cofactor called coenzyme F₄₃₀ (or simply F₄₃₀) that is thought to play an essential role in catalysis (5–7). The crystal structure(s) of MCR reveals that F₄₃₀ is noncovalently bound to MCR and sits at the bottom of a 30 Å hydrophobic channel (8) that is sufficiently deep to accommodate both substrates.

The Ni atom of F₄₃₀ in MCR can exist in three different oxidation states, each exhibiting several coordination states. Active MCR_{red1} contains Ni(I), which is the form that can react with methyl-SCoM to catalyze methane formation (9, 10). In addition to MCR_{red1}, two other states of MCR that could be relevant for the catalytic mechanism are MCR_{ox1} and MCR_{ps}.

On the basis of spectroscopic and computational studies, MCR_{ox1} is best described as a high-spin Ni(II)/thiyl radical that is in resonance with a Ni(III)/thiolate species (11, 12). MCR_{ox1} resembles a proposed catalytic intermediate and is called the “ready state” (9) because it can be converted to MCR_{red1} in vitro by incubation with the low-potential reductant titanium(III) citrate [Ti(III) citrate] (10). MCR_{ox1} is generated in vivo by treating the actively growing cells with sodium sulfide (13) or, alternatively, by switching the gas from an 80% H₂/20% CO₂ mixture to an 80% N₂/20% CO₂ mixture (14). MCR_{ox1} can be generated in vitro by treating MCR_{red2} (MCR_{red1} in the presence of HSCoM and CoBSH) with polysulfide (15).

[†] This work was partly supported by a grant from the Department of Energy (S.W.R., DE-FG03-ER20297) and by an NSF grant (DBI-0552648) that supported D.M.L.’s research as part of a summer REU. The mass spectrometry instrumentation was purchased with funds from an NIH grant (1P20RR17675) to help support the Instrumentation Core of the Redox Biology Center at the University of Nebraska.

* To whom correspondence should be addressed. Phone: (734) 615-4621. Fax: (734) 763-4581. E-mail: sragsdal@umich.edu.

[‡] University of Nebraska.

[§] Current address: Department of Biological Chemistry, MSRB III, 5301, 1150 W. Medical Center Dr., Ann Arbor, MI 48109-0606.

^{||} Simpson College.

¹ Abbreviations: MCR, methyl-coenzyme M reductase; methyl-SCoM, methyl-coenzyme M or 2-(methylthio)ethanesulfonate; HSCoM, coenzyme M or 2-thioethanesulfonate; CoBSH, coenzyme B or *N*-7-mercaptoheptanoylthreonine phosphate; BPS, 3-bromopropane sulfonate; BBS, 4-bromobutane sulfonate; MCR_{red1}, MCR exhibiting the Ni(I) EPR signal; MCR_{ps}, MCR exhibiting the alkyl-Ni(III) signal arising from reaction of MCR_{red1} with BPS; MCR_{BS}, MCR exhibiting the alkyl-Ni(III) signal arising from the reaction of MCR_{red1} with BBS; MCR_{XA}, MCR exhibiting the alkyl-Ni(III) signal arising from reaction of MCR_{red1} with bromocarboxylic acids; NIM, negative ion mode.

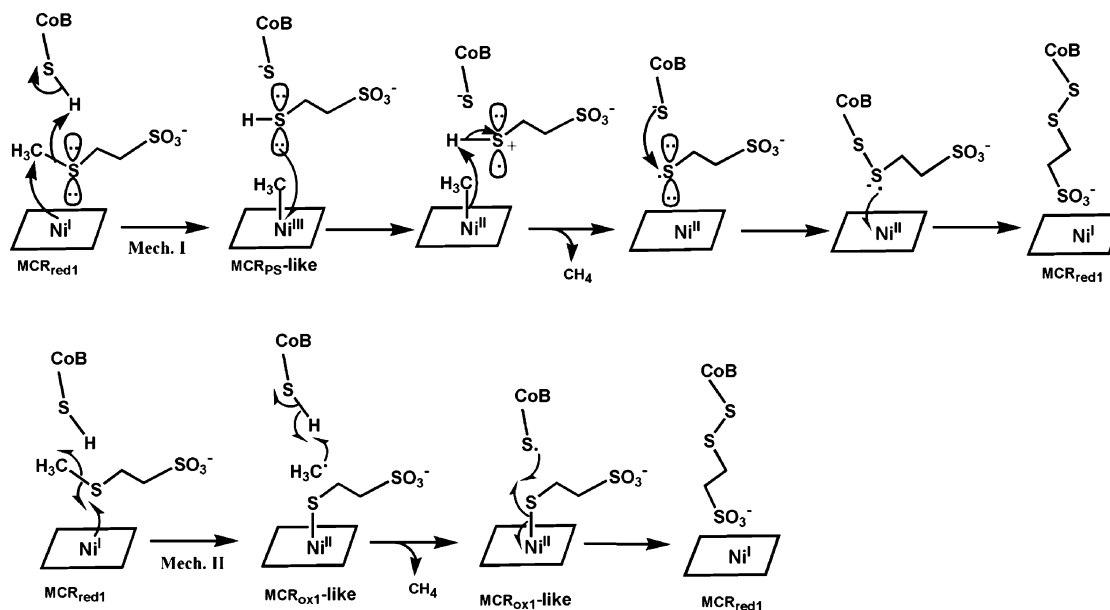


FIGURE 1: Relationship among MCR_{ox1} , MCR_{PS} , and the two proposed mechanisms for MCR.

The second state of MCR that may be relevant for catalysis is MCR_{PS} (formerly MCR_{BPS}) (16). MCR_{PS} has been described as a high-spin Ni^{II} /alkylsulfonate radical species resonating with a Ni^{III} /alkyl species (17, 18) and, thus, resembles the proposed methyl-Ni catalytic intermediate. MCR_{PS} is generated in vitro by incubation of MCR_{red1} with 3-bromopropionate sulfonate (BPS) (16), which is a potent inhibitor (apparent $K_i = 50$ nM) (19, 20) of MCR that also has been classified as an irreversible inhibitor (21). However, when it was recognized that the MCR_{PS} state can be converted back to the active MCR_{red1} state by reacting with thiolates, reversing inhibition, BPS was classified as a reversible redox inactivator (22). Thus, both MCR_{PS} and MCR_{ox1} are ready states that can generate MCR_{red1} in vitro; furthermore, they exhibit similar UV-visible and EPR spectra.

The two mechanisms for methane formation can be distinguished by the first step of catalysis (Figure 1). In mechanism I, which is based on the crystal structure and mechanistic work with F_{430} model complexes (23–25), nucleophilic attack of Ni^{I} - MCR_{red1} on the methyl group of methyl-S-CoM generates a methyl-Ni intermediate (26). Although a true methyl-Ni intermediate has not been described upon reaction of MCR_{red1} with the native substrate methyl-S-CoM, the reaction of BPS and other alkyl halides with MCR_{red1} generates an alkyl-Ni(III) species that is subsequently attacked by free organic thiolates to generate the thioether product and MCR_{red1} (22). This reaction is analogous to that of the reaction catalyzed by methionine synthase, where homocysteine acts as a nucleophile to reduce methyl-Co(III) to form Co(I) and methionine (27).

Mechanism II, which is based on density function theory computations (28, 29), avoids the methyl-Ni species because cleavage of the strong methyl-S bond of methyl-S-CoM to form a relatively weak methyl-Ni(III) species was determined to be extremely endothermic (45 kcal/mol). Therefore, mechanism II proposes attack of Ni^{I} on the sulfur atom adjacent to the methyl group of methyl-S-CoM, resulting in homolytic cleavage of the methyl-sulfur bond

to generate a methyl radical and a Ni^{III} -thiolate \leftrightarrow Ni^{II} -thiol radical complex ($\text{MCR}_{\text{ox1-like}}$ species) (Figure 1).

It was recently shown (22) that the alkyl-Ni(III) species (MCR_{PS}) can be converted to the active MCR_{red1} state when it is reacted with various thiols at pH 10.0. The MCR_{PS} intermediate is chemically similar to the proposed alkyl-Ni intermediate in the first step of mechanism I; however, the position of attack on BPS is stereochemically comparable to the first step in mechanism II. The position of attack by Ni^{I} is probably influenced by the placement of BPS (or other analogues) in the active site. On the basis of the $\text{MCR}_{\text{ox1-silent}}$ crystal structure, the sulfonate group of HSCoM is firmly anchored by three contacts at the “back” of the active site and the thiolate is ligated to Ni. Similarly, the reactivity of CoBSH would be influenced by its location in the substrate channel relative to the position of the Ni-bound ligand. CoBSH has phosphate and carboxylate groups that anchor it to the upper lip of the channel and an alkyl chain that leads into the active site and terminates in a thiol group 8.7 Å from the nickel atom of F_{430} (8).

To improve our understanding of the selectivity of the MCR reaction toward nucleophilic attack by Ni^{I} , one could compare the reactivity of a series of brominated sulfonates of varying chain length. However, such a series of compounds is not commercially available. On the other hand, substitution of the sulfonate of BPS with a carboxylate still allows formation of a $\text{MCR}_{\text{PS-like}}$ signal (22), which we call MCR_{XA} . Furthermore, methylmercaptopropionate is a substrate for MCR ($k_{\text{cat}}/K_M = 26 \text{ M}^{-1} \text{ s}^{-1}$), albeit ~ 110 -fold less reactive than the natural substrate, methyl-S-CoM ($k_{\text{cat}}/K_M = 2.8 \times 10^3 \text{ M}^{-1} \text{ s}^{-1}$) (30), and bromopropionate (like BPS) is an inhibitor (18), indicating that brominated carboxylic acids mimic the interactions of BPS and methyl-S-CoM at the MCR active site. Therefore, to improve our understanding of the selectivity of the MCR reaction, we in this paper compare the reactivity of a series of brominated compounds of varying chain lengths in the formation of the alkyl-Ni(III) complexes and in the subsequent reaction with organic thiol to regenerate the active enzyme.

Here we show that various brominated acids ranging from the relatively small bromobutyric acid (Br4A) to the relatively large bromohexadecanoic acid (Br16A) can all react with MCR_{red1} to form an EPR-active species, MCR_{XA} , that is nearly identical to MCR_{PS} . On the basis of these studies, a model has been proposed for the mode of binding of various brominated acids of different chain lengths that can be classified as (a) methyl-SCoM-like and (b) CoBSH-like. The results provide information about the selectivity of MCR for its substrates (methyl-SCoM, CoBSH, and BPS) and may aid in the development of other substrate analogues or inhibitors of MCR.

MATERIALS AND METHODS

Materials and Organism. *Methanothermobacter marburgensis* (formerly *Methanobacterium thermoautotrophicum* strain Marburg) was obtained from the Oregon Collection of Methanogens (Portland, OR) catalog as OCM82. All buffers, media ingredients, and other reagents were acquired from Sigma-Aldrich (St. Louis, MO) unless otherwise stated and were of the highest available purity. Solutions were prepared using Nanopure deionized water. N_2 (99.98%), H_2S (99.0%), H_2/CO_2 (80%/20%), and Ultra High Purity (UHP) H_2 (99.999%) were obtained from Linweld (Lincoln, NE). Ti(III) citrate solutions were prepared from a stock solution of 200 mM Ti(III) citrate, which was synthesized by adding an aqueous solution of sodium citrate (5.8 g of sodium citrate added to 20 mL of H_2O) to Ti(III) trichloride (30 wt % solution in 2 M hydrochloric acid) (Acros Organics, Morris Plains, NJ) under anaerobic conditions and adjusting the pH to 7.0 with a saturated solution of sodium bicarbonate (31). The concentration of Ti(III) citrate was determined routinely by titrating a methyl viologen solution.

***M. marburgensis* Growth, Harvest, and MCR_{red1} Purification Conditions.** MCR_{red1} was isolated from *M. marburgensis* cultured on a $\text{H}_2/\text{CO}_2/\text{H}_2\text{S}$ mixture (80%/20%/0.1%) at 65 °C in a 14 L fermentor (New Brunswick Scientific Co., Inc., New Brunswick, NJ) (9). Culture media were prepared as previously described (32). MCR_{red1} was generated in vivo and purified as described previously (22). The purification procedure routinely generates 60–70% MCR_{red1} as determined by UV–visible and EPR spectroscopy as described previously (22).

Spectroscopy of MCR. UV–visible spectra of MCR were recorded in the anaerobic chamber using a diode array spectrophotometer (model DT 1000A, Analytical Instrument Systems, Inc., Flemington, NJ). EPR spectra were recorded on a Bruker EMX spectrometer (Bruker Biospin Corp., Billerica, MA), equipped with an Oxford ITC4 temperature controller, a Hewlett-Packard model 5340 automatic frequency counter, and a Bruker gaussmeter. Unless otherwise noted, the EPR spectral parameters included the following: temperature, 70 K; microwave power, 10 mW; microwave frequency, 9.43 GHz; receiver gain, 2×10^4 ; modulation amplitude, 10.0 G; modulation frequency, 100 kHz. Double integrations of the EPR spectra were performed and referenced to a 1 mM copper perchlorate standard.

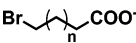
Stopped-Flow Studies. Stopped-flow experiments were performed on an Applied Photophysics (Leatherhead, U.K.) spectrophotometer (SX.MV18) equipped with a photodiode array detector. Rigorous measures were taken to remove

oxygen from the stopped-flow instrument. Buffered solutions of enzymes and inhibitors were made in the anaerobic chamber in 0.5 M Tris-HCl (pH 7.6) containing 0.2 mM Ti(III) citrate at 25 °C. All buffered solutions contained 0.2 mM Ti(III) citrate as an oxygen scavenger, since exclusion of Ti(III) citrate resulted in oxidation of MCR_{red1} . The solutions were then loaded into tonometers, which had been incubated in the anaerobic chamber for at least 4 days and served as reservoirs for the drive syringes of the stopped-flow instrument. The drive syringes and mixing chamber were made anaerobic by flushing the syringe chamber with a 1 mM dithionite/0.02 mM resazurin solution in 0.1 M NaOH. MCR_{red1} and varied concentrations of brominated acids were rapidly mixed at 25 °C in a 1:1 ratio. The reaction was monitored in the single-wavelength mode by following the decrease in the level of MCR_{red1} at 385 nm, and MCR_{XA} formation was followed at 420 nm, with a path length of 1 cm. Data were fit to a single-exponential decay and exponential rise to maximum functions, respectively, using software provided by Applied Photophysics (version SX.MV18) or using Sigma Plot 2001 (Point Richmond, CA). Reported rate constants are the average of at least three different rapid-mixing experiments.

Mass Spectrometry. All mass spectra (LCMS) were collected in negative ion modes by direct infusion to a 4000 Qtrap (ABS) mass spectrometer using a kD Scientific micro flow syringe pump. The data were acquired and processed using Analyst version 1.4.1. Data were acquired in Q1 mode (quadrupole one), and the product ion scan was acquired in the negative ion mode. The mass range of 50–300 amu (atomic mass units) was scanned in 1 s. The ion spray voltage was set to -4500 V; the temperature was set to 22 °C, and the declustering potential (DP) value was -50 V. MCR_{red1} (10 μM) was incubated for 10 min with 2.0 mM 4-bromobutyric acid (Br4A was prepared as a stock solution in 0.1 M formic acid; thus, the final concentration of formic acid in the reaction mixture is 0.4 mM) in 20 mM ammonium carbonate (pH 10.0), and the reaction was followed by UV–visible spectroscopy. For the regeneration of MCR_{red1} from MCR_{XA} with HSCoM, typically 20 μM MCR_{red1} was reacted with 1 mM brominated acid in 50 mM ammonium carbonate (pH 10) to form MCR_{XA} , which was then reacted with 20 mM HSCoM. This reaction was monitored by UV–visible spectroscopy. After MCR_{red1} was fully reactivated, assessed by reaching a stable maximum absorbance of the 385 nm band, the reaction was stopped by freezing the mixture in liquid nitrogen. For analysis, the frozen liquid was thawed, and subsequently, enzyme and ligands were separated using a 0.5 mL Microcon centrifugal filter device with a 30 kDa cutoff filter (Millipore, Billerica, MA). The filtrate containing the product was collected and stored at 4 °C until it was assayed by mass spectrometry. All MS samples were prepared by mixing the ligand solution with an equal volume of acetonitrile.

Reactions between MCR_{red1} and Brominated Acids. MCR_{red1} (typically 0.01–0.02 mM) was incubated in 50 mM Tris-HCl (pH 7.6) at 25 °C for 0.5–2 min, with various brominated acids at concentrations between 0.1 and 2 mM: 0.2 mM 4-bromobutyric acid (Br4A) in formic acid at a final concentration of 0.1 mM, 0.2 mM 5-bromovaleric acid (Br5A), 0.2 mM 6-bromohexanoic acid (Br6A), 1.0 mM 7-bromoheptanoic acid (Br7A) (Karl Industries Inc., Aurora,

Table 1: Kinetic Parameters for the Conversion of MCR_{red1} to MCR_{XA}

chemical name	chemical structure	$\text{MCR}_{\text{red1}} \rightarrow \text{MCR}_{\text{XA}}$ (% conversion) ^a	k_{max} (s ⁻¹)	K_{M} (mM)	$k_{\text{max}}/K_{\text{M}}$ (M ⁻¹ s ⁻¹) ^b
Br4A		85 ± 15	15 ± 0.6	88 ± 5	170 ± 12
	$n = 1$				
Br5A	$n = 2$	56 ± 10	2.0 ± 0.5	65 ± 27	31 ± 15
Br6A	$n = 3$	53 ± 10	0.27 ± 0.05	5.2 ± 3.6	53 ± 38
Br7A	$n = 4$	93 ± 7	2.2 ± 0.3	21 ± 7	140 ± 57
Br8A	$n = 5$	93 ± 1	2.1 ± 0.5	92 ± 34	23 ± 10
Br9A	$n = 6$	60 ± 2	0.074 ± 0.003	1.3 ± 0.2	56 ± 7
Br10A	$n = 7$	12 ± 8	0.050 ± 0.002	2.2 ± 0.5	22 ± 2
Br11A	$n = 8$	<5 (13 ± 5)	380 ± 170	200 ± 110	1900 ± 1300, 1500 ± 80 ^c
Br12A	$n = 9$	<5 (10 ± 5)	0.28 ± 0.02	0.93 ± 0.26	500 ± 92
Br15A	$n = 12$	6 (20 ± 5)	0.26 ± 0.04	0.16 ± 0.11	1600 ± 1000, 470 ± 64 ^c
Br16A	$n = 13$	8 (41 ± 2)	ND	ND	57 ± 18 ^c

^a The % conversion was determined by EPR. The number in parentheses was obtained when the reaction was performed on ice. For details, refer to Materials and Methods. ^b Second-order rate constants were determined by a hyperbolic fit. ^c Second-order rate constants determined by fitting data to a linear equation.

OH, and Matrix Scientific, Columbia, SC), 0.1 mM 8-bromooctanoic acid (Br8A), 0.2 mM 9-bromononanoic acid (Br9A) (Matrix Scientific), 0.2 mM 10-bromodecanoic acid (Br10A) (Matrix Scientific), 1.0 mM 11-bromoundecanoic acid (Br11A) (Fluka, St. Louis, MO), 1.0 mM 12-bromododecanoic acid (Br12A) (Fluka), 1.0 mM 15-bromopentadecanoic acid (Br15A) (Fluka), and 0.5 mM 16-bromohexadecanoic acid (Br16A). All brominated acid solutions, with the exception of Br4A, were made in 100% ethanol. The rate and extent of formation of new MCR_{XA} complexes were measured by EPR spectroscopy (Table 1).

Special precautions were required for working with 4-bromobutyric acid (Br4A). This compound is unstable in neutral and alkaline solutions; therefore, all experiments were performed by dissolving it in 0.1 M formic acid. Attempts to make a solution of Br4A in neutral- or high-pH solutions or in ethanol resulted in degradation of the acid as we inferred by a decrease in the reactivity of Br4A with MCR_{red1} as a function of time.

RESULTS

MCR_{XA} Formation with Brominated Acids, Studied by EPR and UV-Visible Spectroscopy. Kinetic and spectroscopic studies indicate that, when MCR_{red1} reacts with BPS, bromide is eliminated to generate a six-coordinate Ni(III) complex with propylsulfonate as the upper axial ligand, which undergoes protonation to form propanesulfonate (17, 18, 22). This reaction is analogous to the reaction of MCR_{red1} to generate a methyl-Ni(III) intermediate in methane formation with the natural substrate, methyl-SCoM. Here we expand on a previous study to determine the range of BPS analogues that are accommodated by MCR (22). Instead of sulfonates, we used a series of commercially available brominated carboxylic acids. As described in the introductory section, we hypothesized that the reaction between MCR_{red1} and brominated acids is similar to that with BPS. To test this hypothesis, EPR and UV-visible spectroscopies were used to observe the formation of the Ni(III)-alkanoic acid complexes, and stopped-flow experiments were conducted to characterize the kinetic parameters for the reactions. Since MCR_{XA} [alkyl-Ni(III)] and $\text{MCR}_{\text{silent}}$ [Ni(II)] exhibit similar UV-visible spectra, unambiguous quantification of the amount of MCR_{red1} and of MCR_{XA} was performed by EPR spectroscopy by comparing the doubly integrated signal

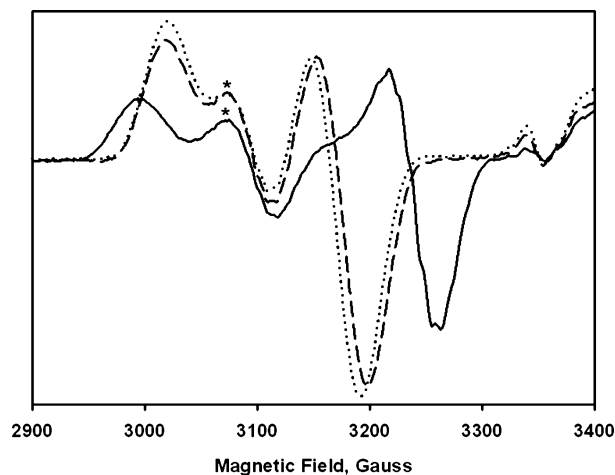


FIGURE 2: EPR spectra showing formation of $\text{MCR}_{7\text{A}}$ from the reaction of MCR_{red1} with Br7A. MCR_{red1} [20.6 μM (—)] was incubated with 1 mM Br7A (---) or 548 μM BPS (···) in 50 mM Tris-HCl (pH 7.6) with 0.1 mM Ti(III) citrate at 20 °C. Asterisks denote contamination from MCR_{ox1} .

intensity with that of a Cu standard. The concentration of $\text{MCR}_{\text{silent}}$ is then equal to the difference between the initial concentration of MCR_{red1} and the amount of MCR_{XA} . Brominated acids used in this study are abbreviated as BrXA, where X refers to the total length of the chain (between 4 and 16 carbons long) including the terminal carboxyl group (A).

MCR_{red1} reacts with brominated acids that are 4–16 carbons in length according to eq 1 to form MCR_{XA} ($X = 4\text{--}16$), which elicits an EPR signal nearly identical to that of MCR_{PS} (Table 1). A representative EPR spectrum of MCR_{red1} and $\text{MCR}_{7\text{A}}$, the product of the reaction between MCR_{red1} and Br7A, is shown in Figure 2.



The near identity of the EPR spectrum of the alkyl-Ni(III) MCR_{PS} state with that of MCR_{XA} strongly indicates that the reaction of MCR_{red1} with the bromo acids also generates an alkyl-Ni(III) species. The different MCR_{XA} complexes accumulate to varying amounts, as reported in Table 1. Those generated from the shorter brominated acids, Br10A and below, form quickly and accumulate to fairly high levels during a 2 min reaction at room temperature. The shortest

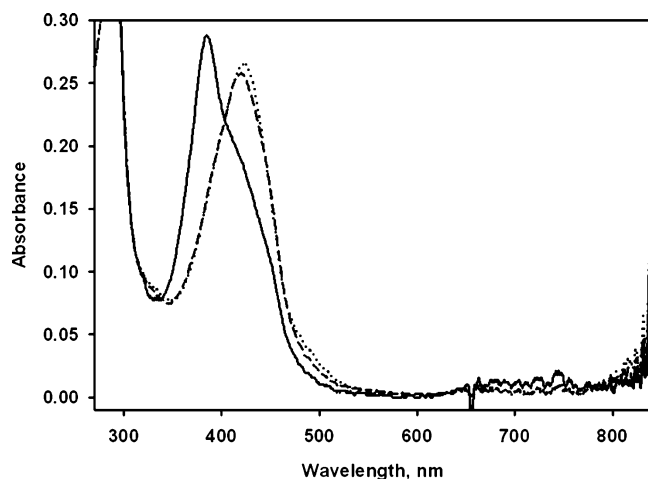


FIGURE 3: UV-visible spectral changes associated with reaction of MCR_{red1} with Br7A and BPS. MCR_{red1} [$8.2 \mu\text{M}$ (—)] was incubated with $400 \mu\text{M}$ Br7A (---) or $219 \mu\text{M}$ BPS (···) in 50 mM Tris-HCl (pH 7.6) with 0.1 mM Ti(III) citrate at 20°C .

acid that was tested was Br4A, which had earlier been reported to form a MCR_{PS} -like species (17, 18, 22). When reacted with MCR_{red1} , Br4A is completely converted to the $\text{MCR}_{4\text{A}}$ species; however, this reaction is unique and is discussed in more detail below. 3-Bromopropionate (Br3A) was not tested, although it has been reported not to form the MCR_{XA} signal (18). Br3A is an analogue of 2-bromoethanesulfonate (BES) and, like BES ($[\text{I}]_{0.5} = 2 \mu\text{M}$), quenches the MCR_{red1} signal by the oxidation of the enzyme from Ni(I) to an EPR-silent Ni(II) state; thus BES and, hence, Br3A appear to act as irreversible inhibitors of MCR (18).

The MCR_{XA} species formed from the longer ($X = 11, 12, 15$, and 16) brominated acids accumulate to a level of less than 10% within 1 min at 25°C , indicating that these complexes form transient species that form and decay more rapidly than the time it takes to hand mix and freeze the samples. When these brominated acids were reacted with MCR_{red1} at 4°C and frozen within $\sim 30 \text{ s}$ in an EPR tube, the extent of accumulation of the corresponding MCR_{XA} species markedly increased (Table 1). We suggest that the MCR_{XA} complexes formed with the longer brominated acids are not well anchored to the active site and, thus, escape from the radical cage and dissociate rapidly from the substrate binding channel in MCR. To improve our understanding of the reactions of MCR_{red1} with the bromo acids, stopped-flow experiments were performed.

Reaction of MCR_{red1} with Brominated Acids and MCR_{XA} Formation Followed by Stopped-Flow Experiments. Formation of the EPR-active MCR_{XA} state is accompanied by a 35 nm red shift relative to MCR_{red1} (Figure 3). Exhibiting absorption maxima at 420 nm , the UV-visible absorption spectra of MCR_{XA} resemble those of MCR_{PS} [alkyl-Ni(III)], MCR_{ox1} [RS-Ni(III)], and $\text{MCR}_{\text{silent}}$ [Ni(II)].

Stopped-flow UV-visible spectroscopy was used to obtain kinetic parameters for the reaction of MCR_{red1} with the brominated acids by monitoring the absorption bands at 385 and 420 nm to follow the decay of MCR_{red1} and formation of MCR_{XA} , respectively. For the reaction with each of the brominated acids, the rate constant (k) could be obtained by a single-exponential equation, which adequately fit the data. The rate of decay of MCR_{red1} matches the rate of MCR_{XA} formation, which indicates that there are no intermediates

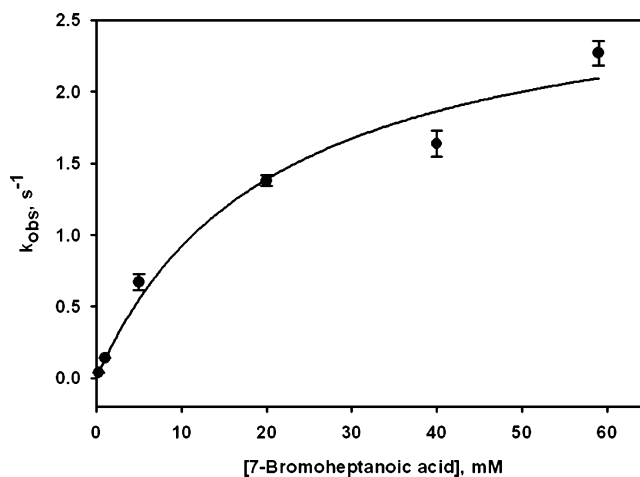


FIGURE 4: Dependence of the k_{obs} for $\text{MCR}_{7\text{A}}$ formation on Br7A concentration. MCR_{red1} ($10 \mu\text{M}$) was converted to $\text{MCR}_{7\text{A}}$ by the addition of different concentrations of Br7A in 0.5 M Tris-HCl (pH 7.6) containing 0.2 mM Ti(III) citrate. The data were fit to a two-parameter hyperbolic equation with a k_{max} of $2.8 \pm 0.4 \text{ s}^{-1}$ and a K_{M} of $21 \pm 8 \text{ mM}$ and a second-order rate constant of $140 \pm 57 \text{ M}^{-1} \text{ s}^{-1}$.

in the conversion of MCR_{red1} to MCR_{XA} or that any intermediates are too transient to be observed. These rate constants were plotted versus the BrXA concentrations to determine the second-order rate constant ($k_{\text{max}}/K_{\text{M}}$) for MCR_{XA} formation as exemplified for Br7A in Figure 4. The second-order rate constants for formation of the MCR_{XA} complexes with the shorter and medium length acids ($X = 5-10$) are between 20 and $60 \text{ M}^{-1} \text{ s}^{-1}$ (Table 1 and Figures S1–S5), with the exception of $\text{MCR}_{7\text{A}}$, which has a second-order rate constant of $140 \text{ M}^{-1} \text{ s}^{-1}$. The second-order rate constants for formation of $\text{MCR}_{11\text{A}}$, $\text{MCR}_{12\text{A}}$, and $\text{MCR}_{15\text{A}}$ (Table 1 and Figures S6–S8) are significantly higher. The k_{max} and K_{M} values for $\text{MCR}_{16\text{A}}$ could not be determined due to solubility issues involved with Br16A concentrations of $>0.5 \text{ mM}$. However, with the available concentrations, a linear fit of the data established a second-order rate constant of $60 \text{ M}^{-1} \text{ s}^{-1}$ (Table 1 and Figure S9).

The kinetics for formation of these MCR_{XA} complexes can be compared to those for formation of their similarly sized sulfonate cousins, MCR_{PS} and MCR_{BS} , and to the rate of methane formation from methyl-SCoM. $\text{MCR}_{4\text{A}}$ is formed with an overall second-order rate constant of $170 \text{ M}^{-1} \text{ s}^{-1}$, which is 1000 times lower than that for formation of MCR_{PS} ($2.3 \times 10^3 \text{ M}^{-1} \text{ s}^{-1}$ at 25°C) (17, 18, 22). However, the k_{max} values for these reactions are nearly identical (17 s^{-1} for MCR_{PS} and 15 s^{-1} for $\text{MCR}_{4\text{A}}$); therefore, the decreased catalytic efficiency of the formation of $\text{MCR}_{4\text{A}}$ relative to MCR_{PS} comes exclusively from the difference in K_{M} values for these two substrates, $\sim 90 \text{ mM}$ for Br4A and $\sim 0.09 \text{ mM}$ for BPS. On the other hand, the $k_{\text{max}}/K_{\text{M}}$ for $\text{MCR}_{4\text{A}}$ formation is only 5.4-fold lower than the $k_{\text{cat}}/K_{\text{M}}$ for methane formation from methyl-SCoM ($930 \text{ M}^{-1} \text{ s}^{-1}$ at 20°C and $1.9 \times 10^4 \text{ M}^{-1} \text{ s}^{-1}$ at 65°C), and the k_{max} value is actually 3-fold higher than the k_{cat} for methane formation at 20°C . The second-order rate constant for $\text{MCR}_{5\text{A}}$ formation ($31 \text{ M}^{-1} \text{ s}^{-1}$) is 70-fold lower than that for formation of MCR_{BS} ($2.3 \times 10^3 \text{ M}^{-1} \text{ s}^{-1}$), the analogous sulfonate complex, resulting from a 7-fold increase in K_{M} and an ~ 10 -fold decrease in k_{max} . The reactions of MCR_{red1} with Br7A and Br8A exhibit kinetic parameters similar to those of the shorter

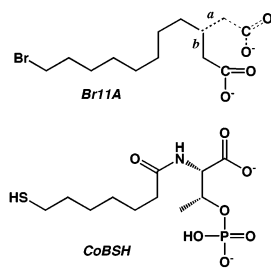


FIGURE 5: Comparison of the structures of Br11A and CoBSH. Two alternative conformations (a and b) are shown with solid and dotted lines.

bromo acids with near or complete conversion to MCR_{7A} and MCR_{8A}. For example, MCR_{7A} formation occurs with a second-order rate constant of 140 M⁻¹ s⁻¹, the k_{\max} values are rather high ($\sim 2\text{--}3$ s⁻¹), and the K_M values are similar to those of methyl-SCoM. We conclude that the short chain brominated acids are positioned in the active site much like methyl-SCoM and HSCoM and react similarly to BPS.

There is a marked drop in both k_{\max} and K_M values for the reactions of MCR_{red1} with Br9A, Br10A, Br12A, Br15A, and Br16A (Table 1 and Figures S4, S5, and S7–S9). The K_M values for most of these Br_XA species fall in the range of the K_M values for CoBSH (~ 0.2 mM) (21), and the values of k_{\max}/K_M for the reactions with Br11A, Br12A, and Br15A are similar to the k_{cat}/K_M values for CoBSH (2.2×10^3 M⁻¹ s⁻¹ at 20 °C) in methane formation (26), suggesting that these long chain bromo acids are recognized by MCR as CoBSH analogues. On the basis of a simple structural analysis using ChemDraw (Figure 5), the negatively charged oxygen on the carboxyl group of Br10A would be in the same position as the carboxylate oxygen of CoBSH and the oxygen from the carboxylate of Br12A would occupy the same position as the phosphate oxygen of CoBSH. The corresponding MCR_{XA} complexes decay more rapidly than those formed from the shorter BPS-like bromo acids, with <10% of the MCR_{XA} complex accumulating when it is mixed at room temperature (Table 1). The yield of EPR-active MCR_{XA} could be increased to $\sim 20\text{--}40\%$ by performing the reaction at 4 °C.

Although Br11A reacts very rapidly with MCR_{red1}, we did not observe saturation even at concentrations of 60 mM; therefore, there is a relatively high standard error associated with both the K_M (200 mM) and k_{\max} (380 s⁻¹) values listed in Table 1. The second-order rate constant for MCR_{11A} formation determined from a linear fit (1500 ± 80 M⁻¹ s⁻¹) is more accurate and is in reasonable agreement with that determined from a hyperbolic fit (1900 M⁻¹ s⁻¹). Due to the low solubility of Br15A and Br16A, kinetic parameters were determined using brominated acid concentrations no greater than 0.5 mM. Regardless, the k_{obs}/K_M values are comparable to that obtained with Br11A; for example, for the reaction of Br15A with MCR_{red1}, the second-order rate constant is 1600 M⁻¹ s⁻¹ (Figure S8). Then, with Br16A, saturation could not be reached and the k_{\max}/K_M value, determined from a linear fit, is 57 M⁻¹ s⁻¹.

Reaction of MCR_{red1} with Br4A: Self-Reactivation of MCR_{4A} To Form MCR_{red1}. When the reaction between MCR_{red1} and Br4A was monitored by UV–visible and EPR spectroscopy, MCR_{red1} was shown to quantitatively convert to MCR_{4A}, as previously described (17, 18, 22); however,

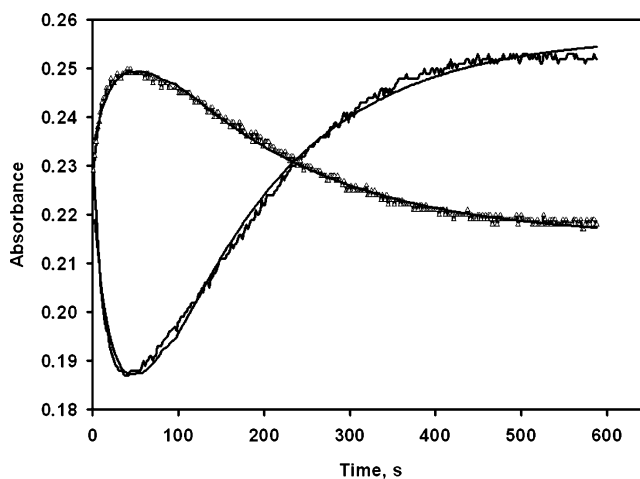


FIGURE 6: Formation of MCR_{4A} followed by regeneration of MCR_{red1}. The formation or decay of MCR_{4A} and MCR_{red1} was monitored at 385 nm (—) and 420 nm (---) by UV–visible spectroscopy. MCR_{red1} (10 μ M) was reacted with 0.2 mM Br4A in 200 mM ammonium carbonate (pH ~ 10). The data were fit to three-component sequential equations with the following parameters: for the absorbance changes at 385 nm, $k_1 = 0.037 \pm 0.003$ s⁻¹ and $k_2 = 0.0067 \pm 0.0003$ s⁻¹; and for the absorbance changes at 420 nm, $k_1 = 0.036 \pm 0.0010$ s⁻¹ and $k_2 = 0.0054 \pm 0.0007$ s⁻¹.

when lower concentrations (~ 0.2 mM) of Br4A were used, a rapid decrease in absorbance at 385 nm due to formation of MCR_{4A} was observed, followed by a gradual increase in absorbance at 385 nm after ~ 1 min (Figure 6), which corresponds to the re-formation of MCR_{red1}. The regeneration of MCR_{red1} occurred at either pH 10.0 or 7.6 in the absence of free thiols, which were shown to convert MCR_{PS} to MCR_{red1} at pH 10.0 (17, 18, 22).

The rate of MCR_{4A} generation depends on the Br4A concentration, with a second-order rate constant of 170 ± 12 M⁻¹ s⁻¹ ($k_{\max} = 15$ s⁻¹; $K_M = 89$ mM) (Figure S10), while the rate constant for regeneration of MCR_{red1} (0.0067 s⁻¹) is 2200-fold slower and is independent of the Br4A concentration. At low concentrations of Br4A (i.e., 0.2 mM), there is complete (100%) conversion of MCR_{4A} to MCR_{red1} (Figure 6). However, at higher concentrations of Br4A, MCR_{4A} is only partially converted to MCR_{red1}, and at Br4A concentrations greater than 8 mM, there is no appreciable regeneration and the absorbance at 420 nm increases to a limiting value in a single-exponential fashion. The apparent conundrum is that conversion of alkyl-Ni(III) to Ni(I) and an alkane requires the input of two electrons into the Ni(III) center and no redox mediators are present; thus, it was important to determine the product of this MCR_{red1} regeneration reaction.

Mass Spectrometric (MS) Evidence for Formation of an Ester from the Self-Reactivation Reaction of MCR_{4A}. Mass spectrometry was used to identify the product of the self-reactivation reaction of MCR_{red1} with Br4A (Figure 7). In the negative ion mode (NIM), the major peak has an m/z value of 250.8. This corresponds to the molecular formula C₈H₁₃O₄Br with an exact mass of 252, which can be assigned to the bromo carboxy ester, 4-(4-bromobutanoyloxy)butanoic acid, Br-(CH₂)₃-COO-(CH₂)₃-COOH. In NIM, the loss of a proton from the carboxylic terminal group of the bromo-carboxy ester product, Br-(CH₂)₃-COO-(CH₂)₃-COOH, will give the expected m/z value of 251, i.e., $(252 - 1)/1$, consistent with the experimentally observed value (inset of

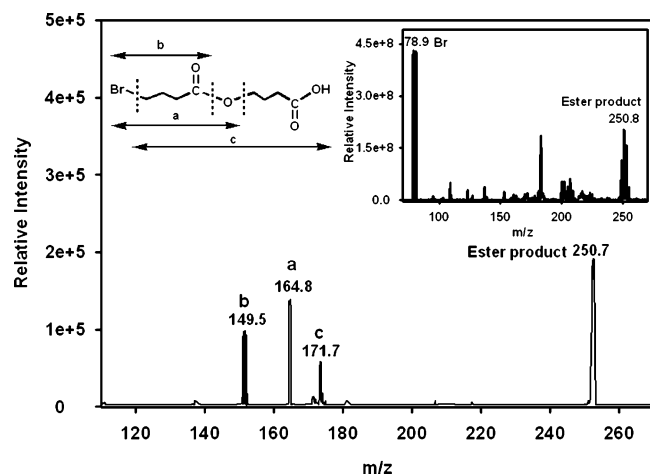


FIGURE 7: NIM MS/MS identification of the fragmented/daughter ions from the bromocarboxy ester product formed from the self-reactivation of MCR_{4A} to MCR_{red1} . MCR_{red1} ($10 \mu\text{M}$) was reacted with 2.0 mM Br_4A in 20 mM ammonium carbonate ($\text{pH} \sim 10$). The inset shows the NIM MS/MS identification of the bromocarboxy ester product formed from the self-reactivation of MCR_{4A} to MCR_{red1} .

Figure 7). Confirmation that the product is the ester was obtained by MS/MS analysis of the parent ion peak (m/z 250.8).

Daughter ion peaks were primarily observed at m/z 149.5, 164.8, and 171.7 (Figure 7). The peak at m/z 171.7 arises from loss of bromine from the parent ion to give $\text{C}_8\text{H}_{13}\text{O}_4$, with an exact mass of 173.2, followed by deprotonation of the carboxylic acid to give the negative ion, $[\text{C}_8\text{H}_{13}\text{O}_4]^-$, with a calculated m/z of 172 [i.e., $252 - 79 = (173 - 1)/1 = 172$], the fragment labeled c in Figure 7. Thus, the ester can cleave at different positions marked a, b, and c (Figure 7) to form daughter ions having molecular formulas of $\text{C}_4\text{H}_6\text{O}_2\text{Br}$, $\text{C}_4\text{H}_6\text{OBr}$, and $\text{C}_8\text{H}_{13}\text{O}_4$, respectively, and the peaks marked a and b agree with the experimentally observed m/z values of 164.8 and 149.5, respectively.

When the negative control experiment was performed in the absence of enzyme, the product was not observed in either NIM or positive ion mode (PIM); however, a peak corresponding to the bromide was observed in NIM, and the remaining fragment after debromination, which presumably is a positive species, was observed in PIM. Thus, the reaction of MCR_{red1} with Br_4A generates the alkyl-Ni(III) species MCR_{4A} . Another molecule of Br_4A reacts with MCR_{4A} to generate the ester, 4-(4-bromobutanoyloxy)butanoic acid. Two possible mechanisms by which this condensation could occur are considered in the Discussion.

MCR_{XA} Is Reactivated to MCR_{red1} by Thiols. It has been recently observed that the MCR_{PS} complex can be reconverted to active MCR_{red1} by nucleophilic attack of various thiolates on the carbon bound to nickel. To determine if MCR_{XA} reacts similarly with thiols, we incubated the MCR_{XA} complexes with HSCoM and followed the decrease in the absorbance of MCR_{XA} at 420 nm and the increase in the absorbance of MCR_{red1} at 385 nm (Figure 8). Since MCR_{XA} and MCR_{silent} have similar UV-visible spectra, we also followed the reaction by EPR spectroscopy (inset, Figure 8).

The rate constant for conversion of the different MCR_{XA} species to MCR_{red1} is in the range of $0.003\text{--}0.012 \text{ s}^{-1}$

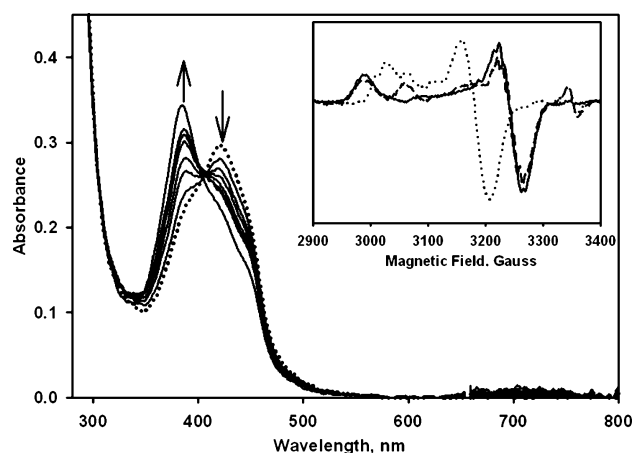


FIGURE 8: UV-visible spectral changes associated with the regeneration of MCR_{red1} from MCR_{7A} incubated with 20 mM HSCoM. MCR_{red1} [$11.52 \mu\text{M}$ (—)] was treated with $100 \mu\text{M}$ Br_7A (···), and the MCR_{7A} formed was incubated with 20 mM HSCoM in 1 M TAPS-Na ($\text{pH} \sim 10$) at 20°C and the absorbance recorded every 6 min for more than 40 min. The inset shows representative EPR spectra of MCR_{red1} (—) MCR_{7A} (···), and the conversion of MCR_{7A} to MCR_{red1} (— — —).

Table 2: Regeneration of MCR_{red1} from MCR_{XA} Using 20 mM HSCoM^a

chemical name	reactivation of MCR_{XA}	$\text{MCR}_{XA} \rightarrow \text{MCR}_{red1}$ (% reactivation) ^b	k_{obs} (s^{-1})
Br5A	yes	46	0.012 ± 0.001
Br6A	yes	65	0.006 ± 0.001
Br7A	yes	81	0.006 ± 0.001
Br8A	yes	31	0.003 ± 0.001
Br9A	no	negligible	NA

^a Experiments were performed in 0.5 M TAPS ($\text{pH} 10$) at 25°C .

^b The % reactivation represents the percent conversion of MCR_{XA} to MCR_{red1} . For details of the experimental conditions, refer to the Materials and Methods.

(Table 2), which is similar to the rate constant for regeneration by HSCoM of MCR_{BS} (k_{max} of 0.006 s^{-1}) and MCR_{PS} (k_{max} of 0.011 s^{-1}). We did not observe a HSCoM concentration dependence for the rate of conversion of MCR_{XA} to MCR_{red1} ; however, the reactions with MCR_{BS} [$K_M = 17 \text{ mM}$ (Figure S11)] and MCR_{PS} [$K_M = 2.8 \text{ mM}$ (21)] exhibit clear hyperbolic binding curves.

Among the different brominated acids listed in Table 2, the percent conversion of MCR_{XA} to MCR_{red1} varies, with a maximum of $\sim 80\%$ conversion of MCR_{7A} to MCR_{red1} (inset, Figure 8). Any EPR-inactive Ni species that is formed most likely decayed into $\text{Ni(II)-MCR}_{silent}$. Furthermore, we did not observe conversion of MCR_{XA} , formed from the longer brominated acids (9-, 10-, 11-, 12-, 15-, and 16-BrA), to MCR_{red1} when these MCR_{XA} species are incubated with HSCoM. Perhaps the MCR_{XA} complex formed from the longer acids did not reactivate because the active site may be plugged, preventing access of thiols to the active site.

Mass Spectrometry Evidence that a Thioether Product Is Formed from the Reaction of MCR_{XA} and HSCoM. We used MS in NIM to identify the product of the reaction between MCR_{5A} and HSCoM as CoM-S-5A, with an m/z value 241.3, which corresponds to the molecular formula $\text{C}_7\text{H}_{14}\text{O}_5\text{S}_2$ with an exact mass of 241.3 after loss of a proton (inset, Figure 9). This assignment was confirmed by MS/MS analysis of the parent ion peak at m/z 241.3, which yields the fragmentation pattern shown in Figure 9.

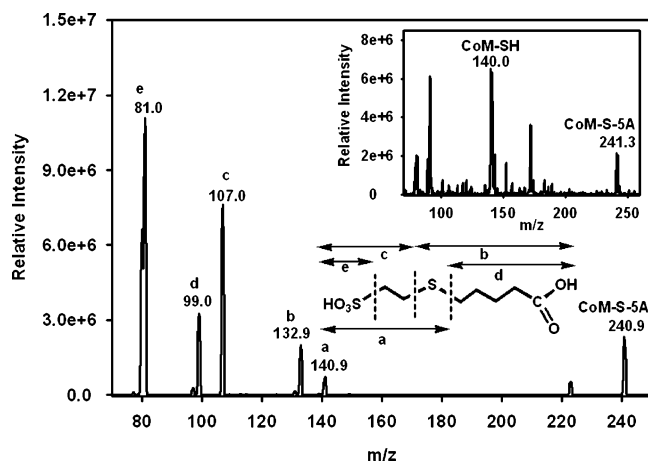


FIGURE 9: NIM MS/MS spectrum of the product of the reaction of MCR_{5A} with HSCoM . MCR_{red1} ($20\ \mu\text{M}$) was reacted with $1\ \text{mM}$ Br5A to form MCR_{5A} , which was reacted with $1\ \text{mM}$ HSCoM in $500\ \text{mM}$ ammonium carbonate ($\text{pH} \sim 10.0$). The inset shows the original NIM MS spectrum of the reaction product.

Daughter ion peaks were observed at m/z 140.9, 132.9, 107.0, 99.0, and 81.0. The daughter ion at m/z 132.9, labeled b, is assigned to the 5-thiopentanoic acid fragment, with the molecular formula $\text{C}_5\text{H}_9\text{O}_2\text{S}$ in which the C–S bond is cleaved. The remaining fragment ion is desulfo-CoM with the molecular formula $\text{C}_7\text{H}_4\text{SO}_3$ and an m/z value of 107.0 (fragment labeled c). The daughter ion peak at m/z 140.9 (peak labeled a) corresponds to $\text{C}_7\text{H}_6\text{O}_3\text{S}_2$ with an exact mass of 141.97, which is formed when the thioether (S–C) bond is cleaved on the pentanoic acid side of the thioether group. A secondary ion that is generated from this S–C fragmentation is pentanoate, with an m/z value of 99.0 (fragment and peak labeled d). The peak at m/z 81.0, labeled e, is assigned to the sulfonate group that is cleaved from various ions.

A negative control experiment performed in the absence of enzyme gave a peak at m/z 242.3, which is only one mass unit higher than that of the expected product (CoM-S-5A , m/z 241.3). To confirm if the m/z 242.3 peak corresponds to the product, MS/MS analysis was performed; the resulting fragmentation pattern was not consistent with that observed for the CoM-S-5A product, which rules out the possibility of the thioether product in the absence of enzyme.

MS coupled with MS/MS also verified formation of the thioether products from the reactions of MCR_{6A} and MCR_{7A} with HSCoM . Thus, the MS data reveal that the reaction of HSCoM with MCR_{XA} generates a thioether product, like the reaction with MCR_{BS} and MCR_{PS} .

DISCUSSION

We studied the reaction of MCR_{red1} with a series of brominated carboxylic acids by EPR and UV–visible spectroscopy and by kinetics. These reactions, as with BPS, apparently involve nucleophilic attack of $\text{Ni(I)-MCR}_{\text{red1}}$ on the terminal carbon adjacent to the bromine atom to eliminate bromide and generate the EPR-active MCR_{XA} species. Compounds that give rise to the MCR_{XA} EPR signal can be abbreviated as BrXA and are generalized by the structure $\text{Br}-(\text{CH}_2)_{3-15}-\text{COO}^-$, where X is the alkyl linker and is ~ 3 –15 carbons long and A is the terminal anionic carboxylate group. On the basis of the near identity of the MCR_{XA} EPR signal to that of MCR_{PS} (21), we can confidently assign

MCR_{XA} as a $\text{Ni(III)-alkyl carboxylate}$. As with MCR_{PS} , the lack of detectable hyperfine splitting from the bromide ($I = 3/2$) demonstrates that it is not near the paramagnetic center, suggesting that the bromide undergoes elimination in the formation of the MCR_{XA} state.

The BrXA species were characterized by their reactivity with MCR_{red1} to form MCR_{XA} (Table 1), by their ability to accumulate MCR_{XA} (Table 1), and by the rate at which the respective MCR_{XA} complexes react with thiolates ($-\text{SCoM}$) to form MCR_{red1} and the CoMS-XA thioether (Table 2). Accumulation of MCR_{XA} (in the absence of the thiolate) is a function of the rate of MCR_{XA} formation and its decay to form XA and the EPR-silent $\text{Ni(II) MCR}_{\text{silent}}$ state. All of these bromo acids form EPR-active MCR_{XA} species and fall into two classes, based on their reactivity (Figure S12).

The shorter brominated acids, Br4A – Br8A , react rapidly with MCR_{red1} to form the MCR_{XA} state, exhibit high values of K_M and k_{max} for MCR_{XA} formation, and accumulate nearly quantitatively in this state; furthermore, these compounds react with HSCoM to form a thioether and regenerate MCR_{red1} . These properties indicate that the short bromo acids mimic binding of methyl- SCoM [$K_M = 5.0\ \text{mM}$ (31)], with their carboxylate groups interacting with Arg120.

The MCR_{4A} complex formed from the short bromo alkanic acid, Br4A , undergoes conversion to MCR_{red1} in the absence of thiolate. One would expect Br4A to be reactive, since like BPS (the most potent inhibitor of MCR), its bromide is adjacent to an electrophilic carbon atom that is four bonds ($\sim 4.8\ \text{\AA}$) from the negatively charged oxygen of the carboxylate. Accordingly, the k_{max} values for formation of MCR_{PS} and MCR_{4A} are nearly identical ($\sim 15\ \text{s}^{-1}$). Therefore, we propose that MCR_{red1} reacts with Br4A to form MCR_{4A} , an alkyl- Ni(III) species, as with the other brominated substrate analogues. However, unlike BPS, with three oxygen atoms on the sulfonate that firmly anchor it to the active site, the carboxylate of Br4A is short of one oxygen and thus would be held by weaker interactions (as indicated by its high K_M value). Regardless, it is likely that the alkanate group is positioned in the active site with the methylene group bound to Ni and the carboxylate group bound to Arg120. Then, two pathways could be considered for formation of 4-(4-bromobutanoyloxy)butanoic acid, the product that is observed by mass spectrometry. In pathway I, a second molecule of Br4A could enter the active site and nucleophilically attack the nickel-bound electrophilic carbon-4 to form the bromocarboxy ester and MCR_{red1} . The nucleophilic attack of the second Br4A is similar to the reaction of HSCoM on the MCR_{XA} species (where $X = 5$ –8). In fact, the rate constants for formation of the thioethers and the bromocarboxy ester are similar. Another possibility, shown in pathway II (Figure S13), is that the electrophilic methylene group bound to Ni in MCR_{4A} could undergo intramolecular attack by the negatively charged oxygen of the carboxylate to form a five-membered butyrolactone and MCR_{red1} . Then, another molecule of Br4A would react with the butyrolactone in solution or in the enzyme active site to generate the bromocarboxy ester.

The longer bromo acids, Br9A – Br16A , apparently mimic CoBSH [$K_M = 0.2\ \text{mM}$ (21)] since they bind more tightly to MCR, exhibit second-order rate constants for formation of MCR_{XA} that are similar to those for CoBSH in methane synthesis, and accumulate to a much lower extent than the

shorter brominated acids. These compounds likely bind with their carboxyl group interacting with the solvent and the positively charged residues at the upper lip of the channel with the bromoalkyl chain reaching toward the nickel center, where it could react rapidly and form the MCR_{XA} complex. The unstable alkyl-Ni(III) complex then rapidly decays to an EPR-silent Ni(II) state. Perhaps this is due to homolytic cleavage of the nickel carbon bond, giving $\text{Ni(II)-MCR}_{\text{silent}}$ and the corresponding alkanolic acid radical, which could abstract a hydrogen atom from the environment of the protein to form the alkanolic acid (21).

CONCLUSION

These studies reveal that MCR_{red1} can react with a wide range of brominated acids giving rise to an alkyl-Ni(III) complex, called MCR_{XA} , which exhibits UV-visible and EPR spectra that are nearly identical to those of the Ni(III)-alkylsulfonate species formed from MCR_{PS} . Thus, the MCR_{XA} complex resembles the methyl-nickel(III) species in the first step of one of the mechanisms (mechanism I) proposed for formation of methane from the natural substrates. These studies reveal the flexibility of the active site of MCR in accommodating a broad array of substrates. The stable MCR_{XA} species (where $X = 5-8$) can undergo attack by nucleophilic thiols to form a thioether product and regenerate the active Ni(I) MCR_{red1} state, while $\text{MCR}_{4\text{A}}$ converts to MCR_{red1} in the absence of a thiol. The unexpected reactivity and flexibility of the MCR active site to accommodate a broad range of substrates provide a molecular ruler for the substrate channel in MCR.

ACKNOWLEDGMENT

We thank Dr. Ashraf Raza for assistance in running mass spectrometric experiments.

SUPPORTING INFORMATION AVAILABLE

Thirteen figures showing second-order rate constant determination for the formation of various MCR_{XA} complexes. This material is available free of charge via the Internet at <http://pubs.acs.org>.

REFERENCES

1. Thauer, R. K. (1998) Biochemistry of methanogenesis: A tribute to Marjory Stephenson. 1998 Marjory Stephenson Prize Lecture, *Microbiology* 144 (Part 9), 2377–2406.
2. DiMarco, A. A., Bobik, T. A., and Wolfe, R. S. (1990) Unusual coenzymes of methanogenesis, *Annu. Rev. Biochem.* 59, 355–394.
3. Ellermann, J., Kobelt, A., Pfaltz, A., and Thauer, R. K. (1987) On the role of N-7-mercaptoheptanoyl-O-phospho-L-threonine (component B) in the enzymatic reduction of methyl-coenzyme M to methane, *FEBS Lett.* 220, 358–362.
4. Kruger, M., Meyerdierks, A., Glockner, F. O., Amann, R., Widdel, F., Kube, M., Reinhardt, R., Kahnt, J., Bocher, R., Thauer, R. K., and Shima, S. (2003) A conspicuous nickel protein in microbial mats that oxidize methane anaerobically, *Nature* 426, 878–881.
5. Diekert, G., Jaenchen, R., and Thauer, R. K. (1980) Biosynthetic evidence for a nickel tetrapyrrole structure of factor F430 from *Methanobacterium thermoautotrophicum*, *FEBS Lett.* 119, 118–120.
6. Diekert, G., Klee, B., and Thauer, R. K. (1980) Nickel, a component of factor F430 from *Methanobacterium thermoautotrophicum*, *Arch. Microbiol.* 124, 103–106.
7. Whitman, W. B., and Wolfe, R. S. (1980) Presence of nickel in factor F430 from *Methanobacterium bryantii*, *Biochem. Biophys. Res. Commun.* 92, 1196–1201.
8. Ermler, U., Grabarse, W., Shima, S., Goubeaud, M., and Thauer, R. K. (1997) Crystal structure of methyl-coenzyme M reductase: The key enzyme of biological methane formation, *Science* 278, 1457–1462.
9. Goubeaud, M., Schreiner, G., and Thauer, R. K. (1997) Purified methyl-coenzyme-M reductase is activated when the enzyme-bound coenzyme F430 is reduced to the nickel(I) oxidation state by titanium(III) citrate, *Eur. J. Biochem.* 243, 110–114.
10. Rospert, S., Bocher, R., Albracht, S. P., and Thauer, R. K. (1991) Methyl-coenzyme M reductase preparations with high specific activity from H₂-preincubated cells of *Methanobacterium thermoautotrophicum*, *FEBS Lett.* 291, 371–375.
11. Craft, J. L., Horng, Y. C., Ragsdale, S. W., and Brunold, T. C. (2004) Nickel oxidation states of F(430) cofactor in methyl-coenzyme M reductase, *J. Am. Chem. Soc.* 126, 4068–4069.
12. Harmer, J., Finazzo, C., Piskorski, R., Bauer, C., Jaun, B., Duin, E. C., Goenrich, M., Thauer, R. K., Van Doorslaer, S., and Schweiger, A. (2005) Spin density and coenzyme M coordination geometry of the ox1 form of methyl-coenzyme M reductase: A pulse EPR study, *J. Am. Chem. Soc.* 127, 17744–17755.
13. Becker, D. F., and Ragsdale, S. W. (1998) Activation of methyl-SCoM reductase to high specific activity after treatment of whole cells with sodium sulfide, *Biochemistry* 37, 2639–2647.
14. Albracht, S. P. J., Ankel-Fuchs, D., Böcher, R., Ellermann, J., Moll, J., van der Zwann, J. W., and Thauer, R. K. (1988) Five new EPR signals assigned to nickel in methyl-coenzyme M reductase from *Methanobacterium thermoautotrophicum*, strain Marburg, *Biochim. Biophys. Acta* 955, 86–102.
15. Mahler, F., Bauer, C., Jaun, B., Thauer, R. K., and Duin, E. C. (2002) The nickel enzyme methyl-coenzyme M reductase from methanogenic archaea: In vitro induction of the nickel-based MCR-ox EPR signals from MCR-red2, *J. Biol. Inorg. Chem.* 7, 500–513.
16. Rospert, S., Voges, M., Berkessel, A., Albracht, S. P., and Thauer, R. K. (1992) Substrate-analogue-induced changes in the nickel-EPR spectrum of active methyl-coenzyme-M reductase from *Methanobacterium thermoautotrophicum*, *Eur. J. Biochem.* 210, 101–107.
17. Hinderberger, D., Piskorski, R. P., Goenrich, M., Thauer, R. K., Schweiger, A., Harmer, J., and Jaun, B. (2006) A nickel-alkyl bond in an inactivated state of the enzyme catalyzing methane formation, *Angew. Chem., Int. Ed.* 45, 3602–3607.
18. Goenrich, M., Mahler, F., Duin, E. C., Bauer, C., Jaun, B., and Thauer, R. K. (2004) Probing the reactivity of Ni in the active site of methyl-coenzyme M reductase with substrate analogues, *J. Biol. Inorg. Chem.* 9, 691–705.
19. Ellermann, J., Rospert, S., Thauer, R. K., Bokranz, M., Klein, A., Voges, M., and Berkessel, A. (1989) Methyl-coenzyme-M reductase from *Methanobacterium thermoautotrophicum* (strain Marburg). Purity, activity and novel inhibitors, *Eur. J. Biochem.* 184, 63–68.
20. Brenner, M. C., Zhang, H., and Scott, R. A. (1993) Nature of the low activity of S-methyl-coenzyme M reductase as determined by active site titrations, *J. Biol. Chem.* 268, 18491–18495.
21. Goenrich, M., Duin, E. C., Mahler, F., and Thauer, R. K. (2005) Temperature dependence of methyl-coenzyme M reductase activity and of the formation of the methyl-coenzyme M reductase red2 state induced by coenzyme B, *J. Biol. Inorg. Chem.* 10, 333–342.
22. Kunz, R. C., Horng, Y. C., and Ragsdale, S. W. (2006) Spectroscopic and kinetic studies of the reaction of bromopropanesulfonate with methyl-coenzyme M reductase, *J. Biol. Chem.* 281, 34663–34676.
23. Lahiri, G. K., and Stolzenberg, A. M. (1993) Facile formation of hexahydroporphyrin complexes by reduction of octaethylisobacteriochlorin nickel(II), *Angew. Chem., Int. Ed.* 32, 429–432.
24. Lin, S.-K., and Jaun, B. (1991) Coenzyme F430 from methanogenic bacteria: Detection of a paramagnetic methylnickel(II) derivative of the pentamethyl ester by ²H-NMR spectroscopy, *Helv. Chim. Acta* 74, 1725–1738.
25. Lin, S.-K., and Jaun, B. (1992) Coenzyme F430 from methanogenic bacteria: Mechanistic studies on the reductive cleavage of sulfonium ions catalyzed by F430 pentamethyl ester, *Helv. Chim. Acta* 75, 1478–1490.
26. Horng, Y. C., Becker, D. F., and Ragsdale, S. W. (2001) Mechanistic studies of methane biogenesis by methyl-coenzyme

- M reductase: Evidence that coenzyme B participates in cleaving the C-S bond of methyl-coenzyme M, *Biochemistry* 40, 12875–12885.
27. Banerjee, R., and Ragsdale, S. W. (2003) The many faces of Vitamin-B12: Catalysis by Cobalamin Dependent Enzymes, *Annu. Rev. Biochem.* 72, 209–247.
28. Pelmeshnikov, V., Blomberg, M. R., Siegbahn, P. E., and Crabtree, R. H. (2002) A mechanism from quantum chemical studies for methane formation in methanogenesis, *J. Am. Chem. Soc.* 124, 4039–4049.
29. Pelmeshnikov, V., and Siegbahn, P. E. (2003) Catalysis by methyl-coenzyme M reductase: A theoretical study for hetero-disulfide product formation, *J. Biol. Inorg. Chem.* 8, 653–662.
30. Wackett, L. P., Honeck, J. F., Begley, T. P., Wallace, V., Orme-Johnson, W. H., and Walsh, C. T. (1987) Substrate analogues as mechanistic probes of methyl-S-coenzyme M reductase, *Biochemistry* 26, 6012–6018.
31. Zehnder, A. J., and Wuhrmann, K. (1976) Titanium(III) citrate as a nontoxic oxidation-reduction buffering system for the culture of obligate anaerobes, *Science* 194, 1165–1166.
32. Schonheit, P., Moll, J., and Thauer, R. K. (1979) Nickel, cobalt, and molybdenum requirement for growth of *Methanobacterium thermoautotrophicum*, *Arch. Microbiol.* 123, 105–107.

BI700925N